Chemosphere 278 (2021) 130229

Contents lists available at ScienceDirect

Chemosphere

journal homepage: www.elsevier.com/locate/chemosphere

Nano zero valent iron encapsulated in graphene oxide for reducing uranium

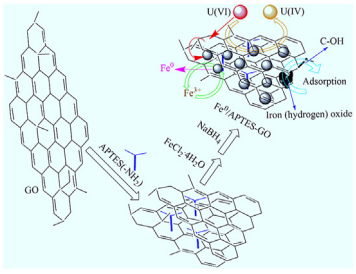
Huiping Tang [a, b, c, 1], Wencai Cheng [a, b, c, 1], Yunpeng Yi [a, b], Congcong Ding [a, b, *], Xiaoqin Nie [a, b, c, **]

[a] Fundamental Science on Nuclear Wastes and Environmental Safety Laboratory, Southwest University of Science and Technology, Mianyang, 621010, China
[b] National Collaborative Innovation Center for Nuclear Waste and Environmental Safety, Southwest University of Science and Technology, Mianyang, 621010, China
[c] School of National Defense Science & Technology, Southwest University of Science and Technology, Mianyang, 621010, China

HIGHLIGHTS

- Maximum removal capacity of Fe^0/APTES-GO for U(VI) reaches 1357.99 mg/g.
- Main removal mechanism of Fe^0/APTES-GO is the reduction of U(VI) to U(IV).
- Fe^0/APTES-GO composites have excellent recycling effect and stability.

GRAPHICAL ABSTRACT



ARTICLE INFO

Article history:
Received 3 December 2020
Received in revised form
28 February 2021
Accepted 6 March 2021
Available online 22 March 2021

Handling Editor: Grzegorz Lisak

Keywords:
Nano zero-valent iron
Uranium
Removal
Graphene oxide

ABSTRACT

Nano zero-valent iron (Fe^0) has been widely used to remove Uranium (U(VI)). In order to enhance the performance of Fe^0 toward U(VI) removal, the Fe^0 was assembled into graphene oxide (GO) sheets via 3-aminopropyl triethoxysilane (APTES) as Fe^0/APTES-GO composites. The Fe^0/APTES-GO composites were triumphantly prepared, characterized and analyzed by means of Scanning Electron Microscope (SEM), Transmission Electron Microscope (TEM) together with Energy Dispersive Spectrometer (EDS), X-ray Diffraction (XRD), Fourier Transform Infrared Spectroscopy (FT-IR) and X-ray Photoelectron Spectroscopy (XPS). SEM and TEM-EDS results manifested that Fe^0 particles were encapsulated into rolled-up GO, which greatly improved the stability of Fe^0. Batch experiment showed that only a small amount of Fe^{2+} was leached in the first two leaching cycles of Fe^0/APTES-GO composites. The removal capacity of Fe^0/APTES-GO composites was up to 1357.99 mg/g at pH = 4.1 and T = 50 °C, which was mainly attributed to the reducing activity of Fe^0 and an abundance of functional groups (i.e., −COOH, C−OH and −OH) on the Fe^0/APTES-GO composites. The electrostatic potential (ESP) from the calculation also supported that U(VI) tended to be reduced at the back side of the GO-Fe^0 cluster.

© 2021 Elsevier Ltd. All rights reserved.

* Corresponding author. Fundamental Science on Nuclear Wastes and Environmental Safety Laboratory, Southwest University of Science and Technology, Mianyang, 621010, China.
** Corresponding author. Fundamental Science on Nuclear Wastes and Environmental Safety Laboratory, Southwest University of Science and Technology, Mianyang, 621010, China.
E-mail addresses: dingc_3650483@163.com (C. Ding), xiaoqin_nie@163.com (X. Nie).
[1] These authors contributed equally to this work and should be considered co-first authors.

https://doi.org/10.1016/j.chemosphere.2021.130229
0045-6535/© 2021 Elsevier Ltd. All rights reserved.

1. Introduction

With the extensive application of uranium resources, uranium pollution is becoming increasingly concentrated by the public. Uranium-containing wastewater produced by uranium industry would flow into human living areas through groundwater, which will seriously damage the health of human beings and surrounding animals (Xiang et al., 2018, 2020; Pirsaheb et al., 2018; Li et al., 2015; Manobala et al., 2020; Xie et al., 2019). Hitherto, the methods to remove U(VI) from aqueous solution include adsorption, membrane separation, extraction, coagulation, ion exchange, bioremediation, chemical precipitation, photocatalysis, flotation, electrochemistry et al. (Manobala et al., 2020; Xie et al., 2019; Li et al., 2018). Some of these methods had their own advantages and had played a huge role in the treatment of uranyl wastewater (Manobala et al., 2020; Xie et al., 2019; Li et al., 2018). But considering the cost, we still have the necessity to find materals for efficiently removal of U(VI) from uranium-containing wastewater.

Nano zero-valent iron (Fe^0) and Fe^0-based materials have been extensively investigated in U(VI) removal, due to their large specific surface area and high reducing reactivity (Xiang et al., 2020; Pirsaheb et al., 2018). Li et al. reported the maximal removal capacity of Fe^0 for U(VI) was 396.37 mg/g (Li et al., 2015). Xiang et al. showed the U(VI) removal capacity of bimetallic Fe^0 particles could reach 575 mg/g (Xiang et al., 2018). However, the rapid oxidation of naked Fe^0 in aqueous solution would hinder its further reducing performance (Xiang et al., 2020; Pirsaheb et al., 2018; Pavelková et al., 2020). In order to improve the utilization efficiency of Fe^0, the methods currently used include vacuum preparation (Pirsaheb et al., 2018), nitrogen or inert gas protection (Sun et al., 2014; Vilardi et al., 2019; Khalil et al., 2018), inorganic coating (Hu et al., 2019a; Liu et al., 2013), electromagnetic field assisted (Pavelková et al., 2020; Srirattana et al., 2017), bacterial synergistic effect (Xiang et al., 2020; Zhao et al., 2020), material support (Raji et al., 2021; Hamd and Dutta, 2020; Ali et al., 2017), organic ligand (Peng et al., 2017, 2021), functionalization (Zhang et al., 2011), modification (Singh et al., 2021), activation (Ye et al., 2021) and emulsion (Dong et al., 2015) methods. Although these methods could improve the utilization efficiency of Fe^0, the environment for the utilization of Fe^0 is harsh and the active life of Fe^0 was usually short under natural conditions.

To overcome this disadvantage, graphene oxide (GO) or GO-based materials have showed their potential as substrates to support and disperse Fe^0, due to the nanosheet structure, abundant functional groups and large surface area (Sun et al., 2014; Wang et al., 2018; Chen et al., 2016; Zhang et al., 2018; Xing et al., 2020; Mehrabi et al., 2019; Hemmat et al., 2020; Farooq et al., 2016; Han et al., 2020; Khoshro et al., 2020; Liu et al., 2019; Lv et al., 2014; Jabeen et al., 2013; Yiming et al., 2018). The Graphene-nZVI (Chen et al., 2016), NZVI/GO (Zhang et al., 2018), GO/nZVI (Xing et al., 2020; Mehrabi et al., 2019), GO@Fe/Cu/Ag (Hemmat et al., 2020) and nZVI-rGO (Farooq et al., 2016) composites were synthesized via chemical process to remove organic pollutants in aqueous solutions and Fe^0 was uniformly dispersed onto GO's surface. The pre-oxidized-NZVI-GO (Han et al., 2020) and nZVI-rGO (Khoshro et al., 2020) composites were prepared through chemical way and showed effective removal for nitrate contaminants. The NZVI/G-Silicon nanocomposites were synthesized via solgel method to remove arsenic (Liu et al., 2019). The nZVI@MG (Lv et al., 2014) and G-nZNI (Jabeen et al., 2013) composites were prepared by chemical method to remediation of Chromium and Lead in wastewater, respectively. The nZVI/rGO compounds were synthesized through chemical deposition method and Fe^0 uniformly dispersed onto the rGO's surface and could remove over 95% of U(VI) ($C_{0\,U(VI)}$ = 0.5 mmol/L) by adsorption and reduction (Sun et al., 2014). The rGO-Polypyrrole-Fe^0 composites were prepared by chemical deposition to remove U(VI) from simulated seawater and the adsorption capacity reached 384.243 mg/g and the removal mechanism was nitrogen's coordination adsorption and reduction to U(IV) insoluble (Yiming et al., 2018). Though these ways extremely enhanced the performance of Fe^0 and inhibited the agglomeration of Fe^0, most of the Fe^0 were exposed on the surface of GO and GO-based materials, which accelerated the oxidation of Fe^0 in natural conditions. To overcome the defect, we chose 3-aminopropyl triethoxysilane (APTES) as crosslinking agent to encapsulate Fe^0 particles inside graphene oxide (GO) (Li et al., 2019). The strategy was to curl GO sheets with the help of APTES, and concurrently encapsulated Fe^0 into the winding GO. The coverage of GO on Fe^0 could effectively reduce the corrosion by water. Meanwhile, the introduction of GO base could lower the agglomeration of Fe^0 particles. The agglomeration of naked Fe^0 particles also hindered their reduction and adsorption performance (Pirsaheb et al., 2018; Zhang et al., 2019a; Loh et al., 2010). GO has good electroconductibility locally at the microscopic level (Li et al., 2018; Jiang et al., 2020), which provides a theoretical basis for the rapid and efficient transfer of electrons from Fe^0 to U(VI). Furthermore, GO is demonstrated to have potential in adsorbing U(VI) (Xie et al., 2019; Ding et al., 2019).

In this study, the GO-loaded Fe^0 was bonded by APTES to form a box-like micro-structure, thus locking Fe^0 into the structure. The goals of this study are 1) to successfully synthesize the Fe^0/APTES-GO composites, 2) to check the performance of Fe^0/APTES-GO in removing U(VI) from water, especially the leaching and cumulative adsorption experiments, 3) to explore the interaction mechanism between Fe^0/APTES-GO and U(VI) from molecular level.

2. Material and methods

2.1. Chemicals

GO was synthesized by Hunmers' method (Stankovich et al., 2006). Some details were listed in the Supplementary Information (SI). Iron chloride tetrahydrate ($FeCl_2{\cdot}4H_2O$, Tianjin guangfu fine chemical research institute, > 99.7%), sodium borohydride ($NaBH_4$, Chengdu kelong chemical reagent factory, > 97%) and 3-Aminopropyl triethoxysilane (APTES, $C_9H_{23}NO_3Si$, >98%) are analytic grade.

2.2. Preparation of Fe^0, Fe^0+GO, Fe^0+APTES and Fe^0/APTES-GO composites

Fe^0 was prepared by redox process. Firstly, add 10 mL $FeCl_2{\cdot}4H_2O$ aqueous solution (0.2 mol/L) into 250 mL three-necked bottle. Afterwards, 10 mL $NaBH_4$ (10.0 mmol/L) was added into the above solution dropwise with magnetic stirring and the protection of $N_{2(g)}$. After 5 h, the black products of Fe^0 were successfully synthesized and separated by centrifuged (5000 r/min), and then washed 3 times with de-ionized water. Eventually, the black solid products Fe^0 were dried in a freeze-dryer for 24 h.

Fe^0+GO and Fe^0+APTES composites were chemically synthesized with the similar procedure of Fe^0. The difference was that 20.0 mL of GO aqueous suspensions (2.0 g/L) and 1 mL APTES were added into the three-necked bottle, respectively before adding the $FeCl_2{\cdot}4H_2O$ aqueous solution.

Fe^0/APTES-GO composites were prepared by chemical approach (Li et al., 2019). 1 mL APTES was firstly added into the 20.0 mL GO aqueous suspensions (2.0 g/L) in three-necked bottle. Afterwards, 10 mL $FeCl_2{\cdot}4H_2O$ aqueous solution (0.2 mol/L) was added into the above mixture with magnetic stirring. Next, 10 mL $NaBH_4$

(10.0 mM/L) was added into the above reaction system dropwise with magnetic stirring. After 5 h, the black products Fe^0/APTES-GO composites were successfully synthesized and separated by centrifuged (5000 r/min), and then washed 3 times with de-ionized water. Finally, the black solid products Fe^0/APTES-GO were dried in a freeze-dryer for 24 h.

2.3. Batch experiments

Batch experiments were conducted with varied initial temperature, pH value and ionic strength under the condition of 0.097 g/L Fe^0/APTES-GO composites and 80 mg/L U(VI). All test samples were prepared at T = 30 °C and pH = 4.1. The reaction time was investigated with U(VI) at pH = 4.1 and T = 30 °C. The Fe^{2+} leaching and the cumulative adsorption were experimented at T = 30 °C and pH 4.1. Ionic strength were performed at T = 30 °C and pH = 3–10. The little volume of 0.01 mol/L Na_2CO_3 or 0.01 mol/L HCl was added to adjust the initial target pH of the solution. Na_2CO_3 was chosen due to the existence of carbonates in groundwater and their remarkable influence on U(VI) species (Xiang et al., 2018). Additionally, Na_2CO_3 could avoid the formation of uranium precipitate at high pH value. To rest the ion strength, NaCl concentration was regulated from 0.01 mol/L to 0.1 mol/L. The adsorption isotherms of U(VI) concentration in the range of 50–200 mg/L were studied at pH = 4.1 and T = 30–50 °C.

2.4. Density functional theory research

Gaussian software was used to do the density functional theory research. During the value of HOMO-LUMO gap process, the theoretical method and basis set that we used were B3LYP/def-TZVP. The data-processing software we used was Multiwfn and VMD software (Lu and Chen, 2011). The electrostatic potential (ESP) on molecular surface also was researched by the Multiwfn and VMD software.

3. Results and discussion

3.1. SEM and TEM analysis

It was very clear that the Fe^0 spheres were covered by the layer of GO from the SEM picture (Fig. 1a). Fe^0 spheres and GO sheets were also obvious on the TEM picture (Fig. 1b). More images of GO and Fe^0/APTES-GO composites could be seen in Figure S1. SEM and TEM pictures revealed that the GO could envelop the Fe^0 spheres with the help of APTES. The corresponding EDS spectra (Fig. 1d) of TEM image in Fig. 1c contained the characteristic carbon element of GO, the characteristic nitrogen element of APTES and iron element. The presence of N element meant that the APTES was involved in the synthesis process of cross-linking GO. The cross-linking GO could provide a micro-cell for Fe^0 in micro-scale and minimize the exposure of Fe^0 to oxygen or active free radical groups in the aqueous solution.

3.2. XRD and FT-IR analysis

The XRD diffraction patterns of Fe^0, Fe^0/APTES-GO and the Fe^0/APTES-GO after reacting with U(VI) were shown in Fig. 2a. Fe^0 appeared its characteristic peaks at $2\theta = 44.7°$ (main diffraction peak) and 65°. We also found the characteristic peaks of Fe^0 in the composites of Fe^0/APTES-GO, which matched with (110) and (200) planes of iron. The crystallinity of Fe^0 on Fe^0/APTES-GO composites decreased as other peaks were not obviously observed (Xiang et al., 2018; Ding et al., 2015a). The XRD results of Fe^0/APTES-GO + U(VI) showed that the peaks of Fe^0 in the composites disappeared. The slightly characteristic peaks of UO_2 at position of 20.8° (main diffraction peak) could match the spectral line well. The tiny peaks of $Fe(OH)_3$ at position of 23.5° (main diffraction peak) were also found in the spectral line. The characteristic peaks of UO_2 and $Fe(OH)_3$ were not obvious, which was due to the poor crystallization of the mixture of Fe^0/APTES-GO + U(VI). The presence of UO_2 indicated that U(VI) was reduced to U(IV) by Fe^0, and concurrently Fe^0 was oxidized to $Fe(OH)_3$. The results were analyzed by using the PDF card of mineral which from the PDF-2 database of the International Center for Diffraction Data. From XRD test results, we knew that the Fe^0/APTES-GO had excellent reducing ability toward U(VI).

Fig. 2b showed the FT-IR spectra of Fe^0/APTES-GO composites and Fe^0/APTES-GO + U(VI) composites. The C=C, C–OH, C–O–C and –OH bonds appeared respectively in FT-IR spectra of Fe^0/APTES-GO at 1634.01, 1384.08, 1028.67 and 3437.40 cm^{-1} (Chen et al., 2015; Huang et al., 2017). When the Fe^0/APTES-GO reacted with U(VI), the –OH bond with a peak value of 3437.40 cm^{-1} was shifted to 3435.31 cm^{-1} and the C=C bond changed from 1634.01 cm^{-1} to 1632.24 cm^{-1} both through stretching vibration (Tsarev et al., 2017). Similarly, peaks at 1384.08 cm^{-1} (C–OH bending) and 1028.67 cm^{-1} (C–O–C stretching) were separately transferred to 1384.38 cm^{-1} and 1048.91 cm^{-1}. These phenomena manifested that C=C, –OH, C–OH and C–O–C bonds were involved in the reaction between Fe^0/APTES-GO and U(VI). In addition, the U–O bond of U(VI) and the U–O bond of U(IV) were separately found in the FT-IR spectrum of Fe^0/APTES-GO + U(VI) at 881.8 cm^{-1} and 480.2 cm^{-1} (Huang et al., 2017; Zhang et al., 2019b). FT-IR results indicated the Fe^0/APTES-GO composites had abundant functional groups which could bind with U(VI). Concurrently, Fe^0/APTES-GO composites could reduce U(VI) to U(IV).

3.3. Effect of reaction time

To investigate the U(VI) removal efficiency of Fe^0, Fe^0+GO, Fe^0+APTES, Fe^0/APTES-GO composites in the water environment, the time curve was shown in Fig. 3a. The removal rate of Fe^0/APTES-GO was the fastest among the Fe^0, Fe^0+GO and Fe^0+APTES and Fe^0/APTES-GO, and the removal capacity was also the highest under the initial conditions of pH = 4.1, T = 30 °C and $C_{0\ U(VI)} = 80$ mg/g. For Fe^0, Fe^0+GO, Fe^0+APTES, the U(VI) removal process could get to about 240 min and removal capacity were 90.359, 155.246, 110.589 mg/g, respectively. For Fe^0/APTES-GO, the U(VI) removal process could fast reach equilibrium in 10 min and keep the maximum removal capacity up to 820 mg/g in the subsequent 10 h. This result indicated that Fe^0/APTES-GO could remove U(VI) faster and more efficiently. Fig. 3b and c showed the experimental kinetics data of U(VI) removal on Fe^0/APTES-GO. Adopting the pseudo-first and pseudo-second order kinetics models to separately simulate the data (added information in the SI). Table 1 displayed the simulatively obtained parameters. The removal of U(VI) by Fe^0/APTES-GO could be better fitted by pseudo-second-order model ($R^2 = 0.999$) than pseudo-first-order model ($R^2 = 0.711$). This result indicated rate-controlled mechanism for U(VI) removal was dominated by chemisorption (Yang et al., 2012).

3.4. Removal isotherms at different temperature

Fig. 4 showed the U(VI) removal by Fe^0/APTES-GO composites under different initial U(VI) concentration (50–200 mg/L) and temperatures (30–50 °C). The removal curve of Fe^0/APTES-GO composites was almost a straight line below U(VI) concentration of 80 mg/L, which was due to that Fe^0/APTES-GO composites could thoroughly remove U(VI) from the aqueous solution. As the temperature rose, the removal capacity increased. The maximum

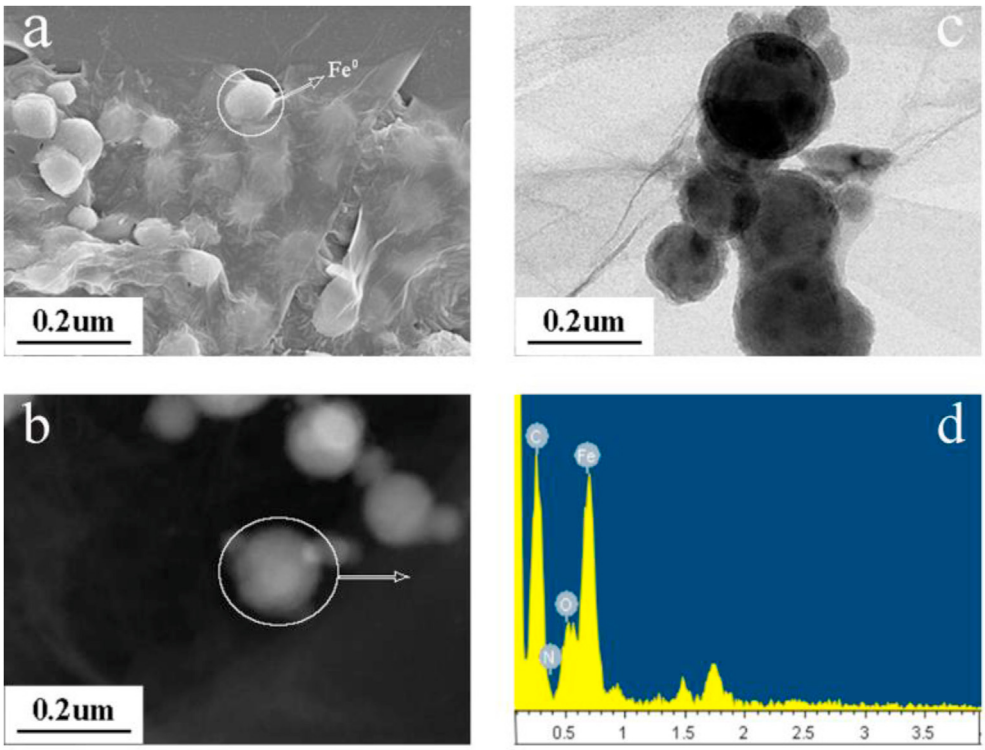


Fig. 1. SEM image of Fe^0/APTES-GO composites (a), TEM image of Fe^0/APTES-GO composites (b) and (c), EDS energy spectrum of Fe^0/APTES-GO composites (d) from Fig. 1(c).

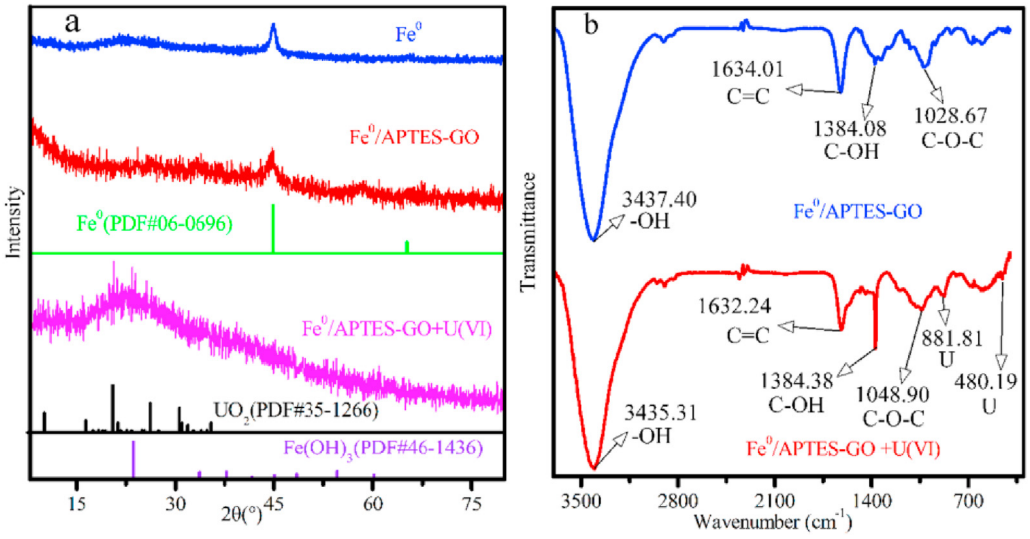


Fig. 2. XRD spectra of Fe^0 and Fe^0/APTES-GO composites before and after reaction with U(VI) (a); FT-IR spectra of Fe^0/APTES-GO composites before and after reaction with U(VI) (b).

removal capacity of U(VI) could reach 1162.6 mg/g, 1197.4 mg/g, and 1357.99 mg/g at 30 °C, 40 °C, and 50 °C under the conditions of pH = 4.1 and reaction 2 h, which was superior to other iron-based adsorbents listed in Table S2. To better understand the removal mechanism, Langmuir and Freundlich equations were used to fit the isotherm (details in SI). Table 2 presented the relevant parameters calculated by the two models. It could be seen from R^2 that the effect of Fe^0/APTES-GO composites removing U(VI) was more suitable for Langmuir model than Freundlich model. These phenomena indicated that the binding energy of the whole surface of Fe^0/APTES-GO composites was uniform. The removal of U(VI) by Fe^0/APTES-GO composites basically was dependent on monolayer sorption but not multilayer sorption (Yang et al., 2012).

3.5. Stability test for U(VI) removal performance

The stability of the adsorbents in solution is a crucial and important index in the future application. Therefore, the Fe^{2+} leaching, cumulative adsorption property and effect of pH ionic strength tests were done by batch experiments. Fig. 5a showed the single Fe^{2+} leaching rate of Fe^0, Fe^0+GO, Fe^0+APTES and Fe^0/APTES-GO of every cycle under the action of 0.1 M HCl. For the pure

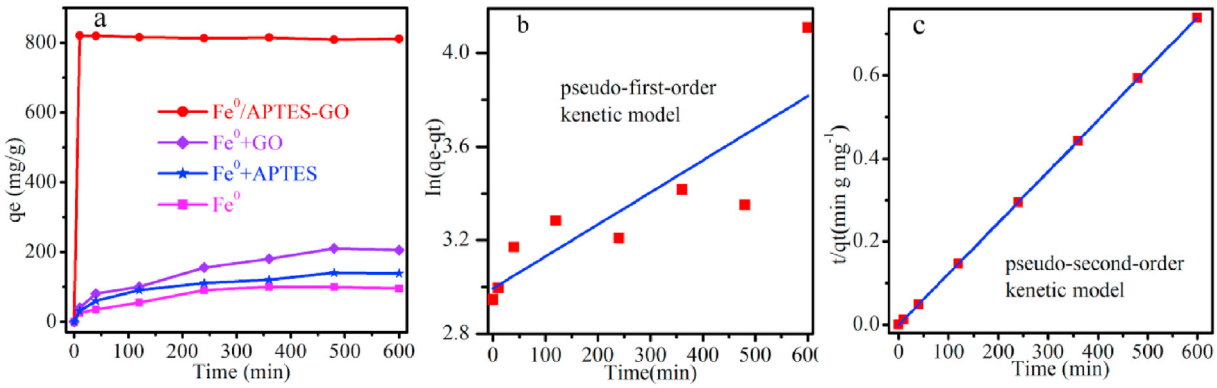


Fig. 3. U(VI) removal by Fe^0/APTES-GO composites, Fe^0+APTES, Fe^0+GO, and Fe^0 as a function of reaction time, $C_{0\ U(VI)}$ = 80 mg/L, pH 4.1 and T = 30 °C (a); simulation of kinetics data of Fe^0/APTES-GO composites by pseudo-first order (b) and pseudo-second order (c) model.

Table 1
Kinetics parameters of U(VI) removal by Fe^0/APTES-GO composites.

Pseudo-first-order model		Pseudo-second-order model	
K_1 (min^{-1})	−0.001	K_2 ($gmg^{-1}min^{-1}$)	0.003
$Q_{e,exp}$ (mgg^{-1})	840.0	$Q_{e,exp}$ (mgg^{-1})	840.0
$Q_{e,cal}$ (mgg^{-1})	20.0	$Q_{e,cal}$ (mgg^{-1})	843.0
R^2	0.711	R^2	0.999

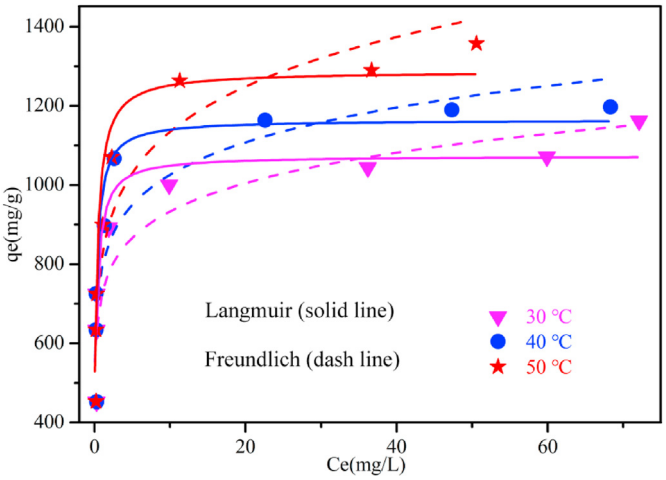


Fig. 4. Removal isotherms of U(VI) by Fe^0/APTES-GO composites under different temperatures; simulation of isothermal data by Langmuir (solid line) and Freundlich (dash line) model.

Table 2
Parameters for Langmuir and freundlich models.

T(°C)	Langmuir			Freundich		
	K_L (Lmg^{-1})	Q_0 (mgg^{-1})	R^2	K_F ($mg^{1-n}L^ng^{-1}$)	n	R^2
30	4.2	1071.1	0.853	730.3	0.11	0.824
40	4.5	1162.0	0.804	796.0	0.11	0.772
50	3.5	1284.4	0.930	826.0	0.14	0.868

Fe^0 sample, the loss quantity of Fe^{2+} reached 70% in the first and second cycles. The Fe^{2+} loss quantity of Fe^0 +GO and Fe^0+APTES samples was ~60% in the first and second cycles. However, only a small amount of Fe^{2+} was detected in the first and second cycles for Fe^0/APTES-GO composites. Even after five times circulation experiment, the leaching amount of Fe^{2+} for Fe^0/APTES-GO composites only reached about 45%. These results indicated that the coverage of GO on Fe^0 could prevent the direct contact between Fe^0 and oxygen or active free radical groups in the aqueous solution, thus maintaining high thermodynamic stability for a long time.

From the view of economic cost and environmental sustainability, it is of significance and necessity to use renewable material. The cumulative adsorption property of Fe^0/APTES-GO composites was tested by the recycling experiment. Fe^0/APTES-GO composites were used to remove U(VI) of 80 mg/L at T = 30 °C and pH = 4.1 every time. Meanwhile, in order to carry out the removal of U(VI) sufficiently, it is of necessity to react for 2 h under the condition of constant temperature oscillation. After the reaction, it was centrifuged, and the separated solid was used for the next removal and repeated five times. The decrease of the performance of Fe^0/APTES-GO composites could be ascribed to the occupation of the reactivity sites by adsorbed U(VI) or precipitation of or UO_2. Fig. 5b showed the relationship between the number of cumulative adsorption and the corresponding U(VI) removal after 6 times, the removal capacity of U(VI) reached 827.767, 815.146, 808.385, 757.211, 659.837 and 508.096 mg/g from once to six times. The removal capacity of U(VI) decreased slightly from 827.767 mg/g to 508.096 mg/g. The slight decrease in removal was attributed to the oxidation of Fe^0 and incomplete desorption of U(VI) from the Fe^0/APTES-GO composites surface. In general, Fe^0/APTES-GO composites had good cumulative adsorption property and supported long-term removal of U(VI) in aqueous solution with low replacement cost.

Fe^0/APTES-GO presented well performance among pH 3−7 with removal capacity of 815 mg/g under the condition of T = 30 °C for 2 h, and pH changed scarcely impacted the performance of Fe^0/APTES-GO. However, the removal performance decreased at pH > 8, which was consistent with other studies (Xiang et al., 2018; Ding et al., 2015a). According to the reported literatures, carbonate had a strong inhibitory effect on the reduction ability of Fe^0 at high pH (Xiang et al., 2018, 2020). Meanwhile, it was reported that negatively charged U(VI)-carbonates like $UO_2(CO_3)_2^{2-}$ and $UO_2(CO_3)_3^{4-}$ dominated at high pH, and they were hard to be bound with negative functional groups of Fe^0 (Xiang et al., 2018; Tsarev et al.,

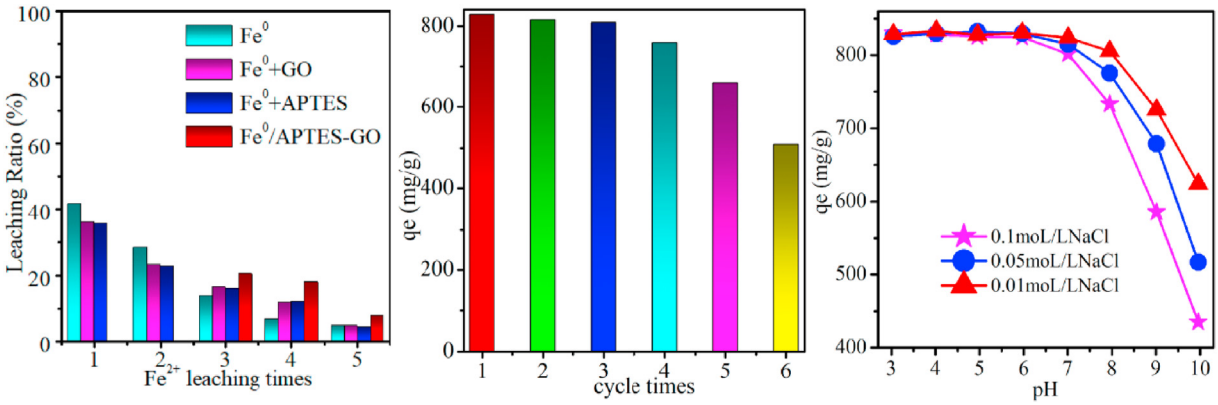


Fig. 5. Test of the stability of Fe^0/APTES-GO composites: leaching of Fe^{2+} (a), cumulative adsorption of Fe^0/APTES-GO composites in the removal of U(VI) (b), and effect of pH and ionic strength ($C_{0U(VI)}$ = 80 mg/L, T = 30 °C) (c).

2017). As shown in Fig. 5c, when pH < 6, the removal performance of Fe^0/APTES-GO was little affected by ionic strength. However, at pH > 6, the removal capacity of U(VI) decreased with the increase of NaCl concentration. This could be due to the electrostatic reaction between Na^+ and the U(VI)-carbonate ions like $UO_2(CO_3)_2^{2-}$ and $UO_2(CO_3)_3^{4-}$ in the solution, which weakened the transfer of U(VI) electrons (Sun et al., 2014; Tsarev et al., 2017). This phenomenon indicated that Fe^0/APTES-GO composites were more suitable to remove U(VI) in acidic solution.

3.6. XPS analysis

Fig. 6 said the XPS patterns of Fe 2p (a), O 1s (b), C 1s (c) of Fe^0/APTES-GO composites before and after reaction with U(VI) and U 4f (d) of after reaction. Fe(III) peaks could be separately fitted at 712.8 eV and 726.4 eV. And the peaks of Fe(II) could be found at 710.5 eV and 724.5 eV. These results could be ascribed to the presence of the surface hydroxides or oxides of Fe(III)/Fe(II), like $Fe(OH)_3$ or Fe_3O_4. Meanwhile, the binding energy of Fe^0 peaks was also observed at 735.2, 719.1 and 706.4 eV (Xiang et al., 2018; Ding et al., 2015a). It was seen from Fig. 6a that the peak value of Fe^0 decreased after reacting with U(VI), especially at 706.3 eV. Meanwhile, the peak of Fe(II) decreased and the peak of Fe(III) increased. These phenomena indicated that U(VI) was reduced to U(IV) by Fe0 and Fe(II). Fig. 6b showed that the peaks of OH^- and O^{2-} of the Fe^0/APTES-GO were fitted at 531.6 eV and 530.6 eV, respectively, in the O 1s spectra (Zhang et al., 2019b; Shenderova et al., 2011). After the Fe^0/APTES-GO composites reaction with U(VI), the peaks of OH^- and O^{2-} severally shifted to 532.1 eV and 530.7 eV. This phenomenon indicated OH^- participated in the U(VI) removal reaction. C 1s spectrum could be simulated by the C—C, C—OH, C—O—C, and —COOH groups at 284.7, 285.8, 286.8 and 288.4 eV (Zhang et al., 2019b; Hu et al., 2019b; Yu et al., 2019) (Fig. 6c). According to the results in Fig. 6c, the C—OH peak at 285.8 eV was changed to 285.5 eV, which could probably be that the functional group C—OH provided adsorption sites for U(VI) when the U(VI) was removed the Fe^0/APTES-GO composites.

In Fig. 6d, the U 4f peaks presented broad U $4f_{7/2}$ and U $4f_{5/2}$ lines separately situated at 382.09 and 392.97 eV. U(VI) peaks could be found in 382.5 and 393.2 eV. The peaks of U (IV) were fitted into 381.7 and 392.5 eV. Synchronously, satellites of U(VI) $4f_{7/2}$ at 394.5 eV (the ΔEs-p of U(VI) of the scope from 9.1 eV to 10.5 eV) and U(IV) at 385.2 eV (the ΔEs-p of U(IV) oxides of scope from 6.6 eV to 7.1 eV) have been discovered (Zhang et al., 2019b; Hu et al., 2019b; Yu et al., 2019). XPS results demonstrated the presence of U(IV), which was accordance with that of XRD and FT-IR. In general, Fe^0/APTES-GO composites reduced U(VI) to U(IV) and precipitated out as UO_2. XPS results showed that U(VI) was the dominant uranium species on the surface of Fe^0/APTES-GO composites materials. The surface functional groups such as —OH, C—OH and —COOH from GO or the corrosion products of Fe^0 could provide adsorption sites for U(VI). In addition to that, U(IV) on the surface of Fe^0/APTES-GO was easily oxidized to U(VI). Both reduction and adsorption contributed to the removal performance of Fe^0/APTES-GO toward U(VI): 1) Fe^0 and Fe(II) provided electrons to reduce U(VI) to U(IV); 2) oxygen-containing groups from GO and iron (hydr)oxides offered sorption sites.

3.7. The value of HOMO-LUMO gap

Theoretical calculation models were established to further interpret the mechanism of the reduction of U(VI) by Fe^0. Fig. 7 showed the HOMO-LUMO gap acquired through different reaction process models. The value of the gap reflected the electroconductibility of the material to a certain extent, and was inversely proportional to the electroconductibility. Fig. 7a and b were the model for the interaction of Fe^0 cluster with GO. When the Fe^0 cluster was in the middle of the GO sheet, the value of HOMO-LUMO gap was 1.9663 a.u. (Fig. 7a). However, when the Fe^0 cluster moved to the edge of the GO sheet, the value of HOMO-LUMO gap reduced to 1.8527 a.u. (Fig. 7b). This meant that U(VI) ion was more easily reduced by Fe^0 cluster at the edges of GO. In most cases, there were more oxygen-containing functional groups in the edge of GO. Thus, a new GO model with —COOH and —OH on its edge was depicted in Fig. 7c, and the value of HOMO-LUMO gap was rapidly dropping to 0.8394 a.u. The electroconductibility was farther boosted by oxygen-bearing function groups. This meant that when U(VI) ion approach to GO, it would easily accept electrons from Fe^0 cluster and be reduced by Fe^0 cluster.

3.8. Electrostatic potential and charge distribution

The electrostatic potential (ESP) on molecular surface was critical for studying and predicting inter-molecular interaction (Murray and Politzer, 2011; Lu and Chen, 2012), and would be helpful for deep understanding the interaction between GO-Fe^0 cluster model and U(VI) ion. Although the trend line was smooth and regular, the negative charge was more concentrated than the positive charge (Fig. 8a). When the Fe^0 cluster moved to the edge of the GO sheet (Fig. 8b), the negative charge was even more concentrated than the positive charge. We also acquired the corresponding ESP-mapped molecule (Fig. 8c and d), and the negative

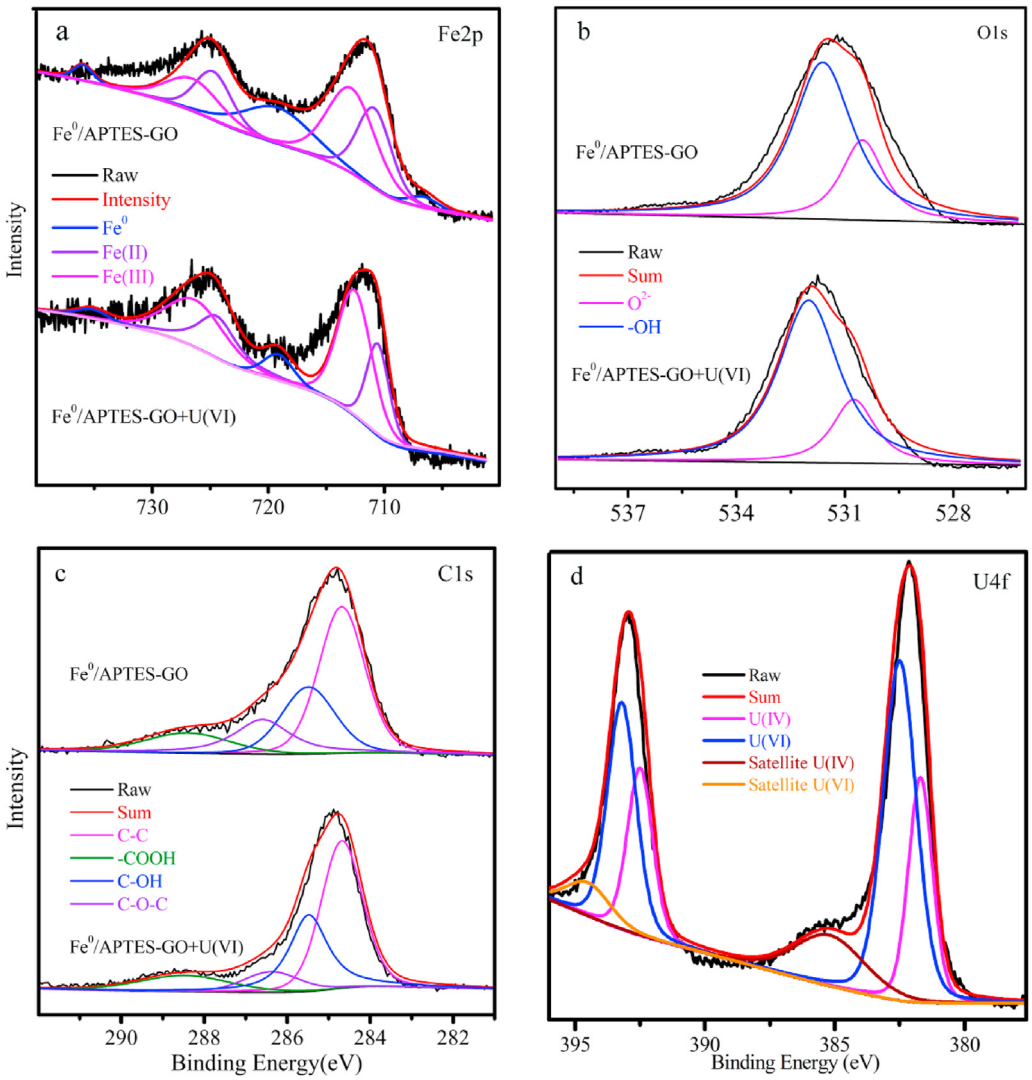


Fig. 6. XPS patterns of Fe 2p (a), O 1s (b), C 1s (c) of Fe^0/APTES-GO composites before (up) and after (down) reaction with U(VI), and U 4f (d) after reaction.

charge was mainly concentrated on the back of GO-Fe^0 cluster. Therefore, when the U(VI) encountered GO-Fe^0 cluster U(VI) tended to bind to the back side of the GO-Fe^0 cluster due to the electrostatic attraction effect. This result provided a visual evidence to deep understand the interaction mechanism between U(VI) and GO-Fe^0 cluster.

3.9. Reaction mechanism

In conclusion, the removal process of U(VI) by Fe^0/APTES-GO composites was a little complicated, which included internal reduction and surface adsorption of composites. The GO films outside of Fe^0/APTES-GO composites not only transferred electrons, but also prevented Fe^0 from coming into direct contact with oxygen or active free radical groups in the aqueous solution, thus prolonging the reduction lifetime of Fe^0 and promoting the reaction of U(VI) reduction to U(IV). The Fe^0 and its Fe(II) oxidation products inside of the Fe^0/APTES-GO composites provided electrons for the reduction of U(VI) to U(IV). The ESP-mapped molecule from the calculation suggested that U(VI) was more readily to bind at the back side of the GO-Fe^0 cluster, where reduction reaction happened via accepting electrons from Fe^0 cluster. As the reaction proceeded, some iron (hydr)oxides like $Fe(OH)_3$ were formed and covered with GO films' surface, which partly hindered the reaction of Fe^0 with U(VI). However, oxygen-containing groups (such as −OH, C−OH and −COOH) from GO and iron (hydr)oxides could offer sorption sites for U(VI). As evidenced by the XRD, FT-IR, XPS and theoretical calculation results and macroscopic measurements, the main way for Fe^0/APTES-GO to remove U(VI) was the reduction of U(VI) to U(IV). Apparently, the adsorption sites were basically derived from the iron (hydr)oxides and GO which were limited. The Fe^0/APTES-GO composites removal capacity was higher than other adsorbents described in previous papers (Li et al., 2015; Xiang et al., 2018; Mahmoud et al., 2017; Ding et al., 2015b, 2015c; Wu et al., 2019; Liu et al., 2021a, 2021b).

4. Conclusions

In this study, Fe^0 particles were loaded inside the slightly rolled GO sheets with the help of APTES. The obtained Fe^0/APTES-GO composites were not only economical and environmentally friendly, but also improved the reduction activity of Fe^0. The maximum removal capacity of U(VI) for Fe^0/APTES-GO composites was 1357.99 mg/g, and the reaction reactivity could keep more than

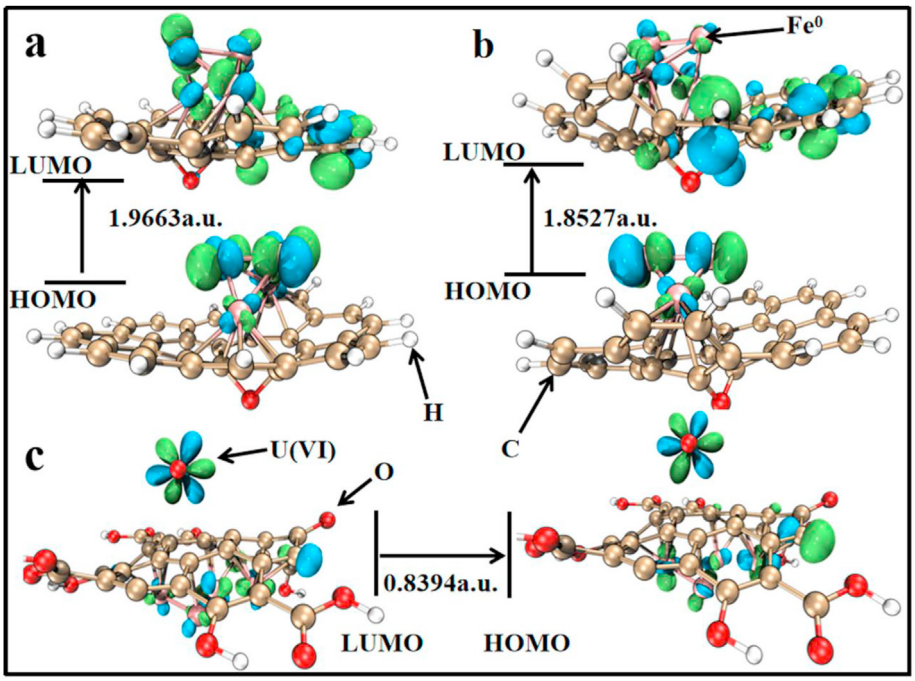


Fig. 7. The value of HOMO-LUMO gap of Fe^0 cluster and GO. Red, gold, white, pink ball represents oxygen, carbon, hydrogen and iron atom, respectively. Petal-shaped orbital atom represents U(VI). (For interpretation of the references to color in this figure legend, the reader is referred to the Web version of this article.)

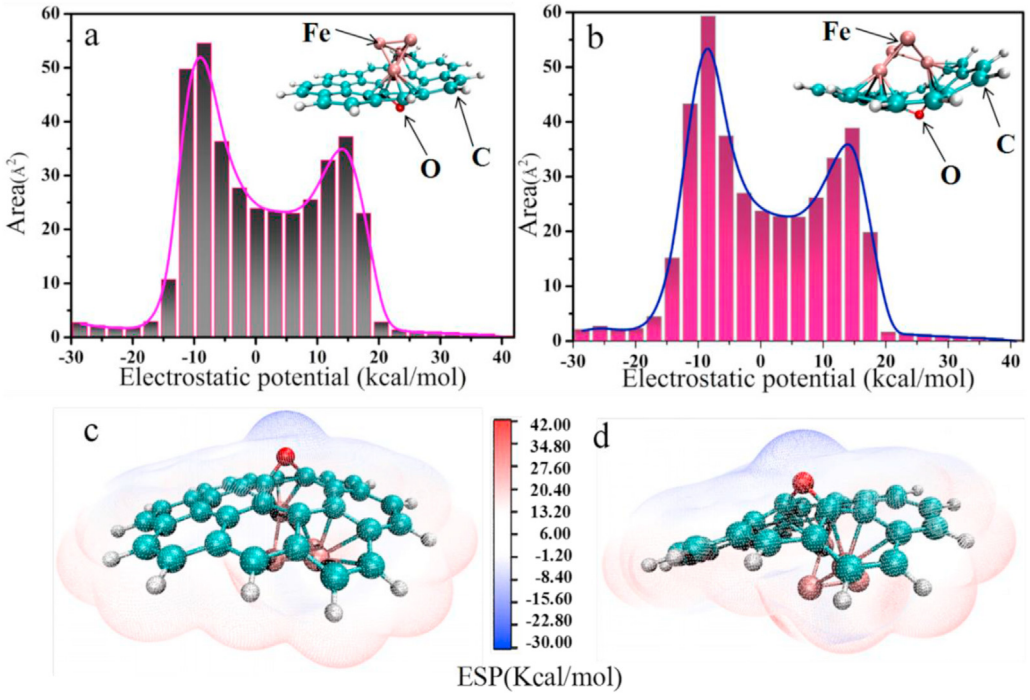


Fig. 8. Surface area in each ESP range on the model surface (a, b) and their corresponding ESP-mapped molecule (c, d): Fe^0 cluster on the center (a, c) and edge (b, c) of GO. Surface negative and positive region of ESP are represented as blue and orange color, respectively. The unit is in kcal/mol. (For interpretation of the references to color in this figure legend, the reader is referred to the Web version of this article.)

for 10 h. In conclusion, Fe^0/APTES-GO composites are stable and can quickly remove U(VI) through reduction and adsorption. Therefore, Fe^0/APTES-GO composites are promising for environmental application. More large-scale tests are needed to further explore the effects of other water quality parameters.

Credit auther statement

Huiping Tang: Methodology, Validation, Formal analysis, Investigation, writing-original and editing. Wencai Cheng: Conceptualization, Software, Formal analysis, Resources, writing-review and editing, Visualization, Project administration, Funding

acquisition. Yunpeng Yi: Validation, Formal analysis, Investigation, Data curation. Congcong Ding: Resources, writing-review and editing, Visualization, Project administration, Funding acquisition. Xiaoqin Nie: Resources, Supervision, Project administration, Funding acquisition.

Declaration of competing interest

The authors declare that they have no known competing financial interests or personal relationships that could have appeared to influence the work reported in this paper.

Acknowledgments

The work was supported by National Natural Science Foundation of China (41703118, 21707110, 41877323); the Foundation of Fundamental Science on Nuclear Waste and Environmental Security Laboratory (17kfhk01); Longshan academic talent research supporting program of SWUST (18LZX 205 and 18LZX 206).

Appendix A. Supplementary data

Supplementary data to this article can be found online at https://doi.org/10.1016/j.chemosphere.2021.130229.

References

Ali, F., Khan, S.B., Kamal, T., Alamry, K.A., Asiri, A.M., Sobahi, T.R.A., 2017. Chitosan coated cotton cloth supported zero-valent nanoparticles: simple but economically viable, efficient and easily retrievable catalysts. Sci. Rep. 7 (1).
Chen, Y., Wang, Y., Zhang, H.B., Li, X., Gui, C.-X., Yu, Z.Z., 2015. Enhanced electromagnetic interference shielding efficiency of polystyrene/graphene composites with magnetic Fe_3O_4 nanoparticles. Carbon 82, 67–76.
Chen, H., Cao, Y., Wei, E., Gong, T., Xian, Q., 2016. Facile synthesis of graphene nano zero-valent iron composites and their efficient removal of trichloronitromethane from drinking water. Chemosphere 146, 32–39.
Ding, C., Cheng, W., Sun, Y., Wang, X., 2015a. Effects of Bacillus subtilis on the reduction of U(VI) by nano-Fe^0. Geochem. Cosmochim. Acta 165, 86–107.
Ding, C., Cheng, W., Jin, Z., Sun, Y., 2015b. Plasma synthesis of β-cyclodextrin/$Al(OH)_3$ composites as adsorbents for removal of UO_2^{2+} from aqueous solutions. J. Mol. Liq. 207, 224–230.
Ding, C., Cheng, W., Sun, Y., Wang, X., 2015c. Novel fungus-Fe_3O_4 bio-nanocomposites as high performance adsorbents for the removal of radionuclides. J. Hazard Mater. 295, 127–137.
Ding, J., Yan, Z., Feng, L., Zhai, F., Chen, X., Xu, Y., Xia, C., 2019. Benzotriazole decorated graphene oxide for efficient removal of U(VI). Environ. Pollut. 253, 221–230.
Dong, J., Wen, C., Liu, D., Zhang, W., Li, J., Jiang, H., et al., 2015. Study on degradation of nitrobenzene in groundwater using emulsified nano-zero-valent iron. J. Nanoparticle Res. 17 (1).
Farooq, U., Danish, M., Lu, S., Naqvi, M., Gu, X., Fu, X., et al., 2016. Synthesis of nZVI@ reduced graphene oxide: an efficient catalyst for degradation of 1,1,1-trichloroethane (TCA) in percarbonate system. Res. Chem. Intermed. 43 (5), 3219–3236.
Hamd, W.S., Dutta, J., 2020. Heterogeneous photo-Fenton reaction and its enhancement upon addition of chelating agents. Nanomaterials for the Detection and Removal of Wastewater Pollutants 303–330.
Han, L., Li, B., Tao, S., An, J., Fu, B., Han, Y., et al., 2020. Graphene oxide-induced formation of a boron-doped iron oxide shell on the surface of NZVI for enhancing nitrate removal. Chemosphere 252, 126496.
Hemmat, K., Khodabakhshi, M.R., Zeraatkar Moghaddam, A., 2020. Synthesis of nanoscale zero-valent iron modified graphene oxide nanosheets and its application for removing tetracycline antibiotic: response surface methodology. Appl. Organomet. Chem. 35, e6059.
Hu, Y., Zhang, M., Li, X., 2019a. Improved longevity of nanoscale zero-valent iron with a magnesium hydroxide coating shell for the removal of Cr(VI) in sand columns. Environ. Int. 133, 105249.
Hu, B., Guo, X., Zheng, C., Song, G., Chen, D., Zhu, Y., et al., 2019b. Plasma-enhanced amidoxime/magnetic graphene oxide for efficient enrichment of U(VI) investigated by EXAFS and modeling techniques. Chem. Eng. J. 357, 66–74.
Huang, W., Cheng, W., Nie, X., Dong, F., Ding, C., Liu, M., et al., 2017. Microscopic and spectroscopic insights into uranium phosphate mineral precipitated by Bacillus mucilaginosus. ACS Earth and Space Chemistry 1 (8), 483–492.
Jabeen, H., Kemp, K.C., Chandra, V., 2013. Synthesis of nano zerovalent iron nanoparticles-Graphene composite for the treatment of lead contaminated water. J. Environ. Manag. 130, 429–435.
Jiang, C., An, D., Wang, Z., Zhang, S., An, X., Bo, J., et al., 2020. A sustainable reduction route of graphene oxide by industrial waste lignin for versatile applications in energy and environment. J. Clean. Prod. 268, 122019.
Khalil, A.M.E., Eljamal, O., Saha, B.B., Matsunaga, N., 2018. Performance of nanoscale zero-valent iron in nitrate reduction from water using a laboratory-scale continuous-flow system. Chemosphere 197, 502–512.
Khoshro, S., Mirbagheri, N.S., Sabbaghi, S., 2020. Removal of nitrate from aqueous solution using nano zerovalent iron-reduced graphene oxide composite: optimization of parameters. Water Environ. J. 1747–6585.
Li, J., Chen, C., Zhang, R., Wang, X., 2015. Nanoscale zero-valent iron particles supported on reduced graphene oxides by using a plasma technique and their application for removal of heavy-metal ions. Chemistry-An Asian Journal 10 (6), 1410–1417.
Li, J., Wang, X., Zhao, G., Chen, C., Chai, Z., Alsaedi, A., et al., 2018. Metal-organic framework-based materials: superior adsorbents for the capture of toxic and radioactive metal ions. Chem. Soc. Rev. 47 (7), 2322–2356.
Li, S.J., Zhou, Y.T., Kang, X., Liu, D.X., Gu, L., Zhang, Q.H., et al., 2019. A simple and effective principle for a rational design of heterogeneous catalysts for dehydrogenation of formic acid. Adv. Mater. 31 (15), 1806781.
Liu, T., Li, X., Waite, T.D., 2013. Depassivation of aged Fe^0 by inorganic salts: implications to contaminant degradation in seawater. Environ. Sci. Technol. 47 (13), 7350–7356.
Liu, P., Liang, Q., Luo, H., Fang, W., Geng, J., 2019. Synthesis of nano-scale zero-valent iron-reduced graphene oxide-silica nano-composites for the efficient removal of arsenic from aqueous solutions. Environ. Sci. Pollut. Control Ser. 26 (32), 33507–33516.
Liu, Y., Pang, H., Wang, X., Yu, S., Chen, Z., Zhang, P., et al., 2021a. Zeolitic imidazolate framework-based nanomaterials for the capture of heavy metal ions and radionuclides: a review. Chem. Eng. J. 406, 127139.
Liu, Y., Huo, Y. zh, Wang, X.X., et al., 2021b. Impact of metal ions and organic ligands on uranium removal properties by zeolitic imidazolate framework materials. J. Clean. Prod. 278, 123216.
Loh, K.P., Bao, Q., Eda, G., Chhowalla, M., 2010. Graphene oxide as a chemically tunable platform for optical applications. Nat. Chem. 2 (12), 1015–1024.
Lu, T., Chen, F., 2011. Multiwfn: a multifunctional wavefunction analyzer. J. Comput. Chem. 33 (5), 580–592.
Lu, T., Chen, F., 2012. Quantitative analysis of molecular surface based on improved Marching Tetrahedra algorithm. J. Mol. Graph. Model. 38, 314–323.
Lv, X., Xue, X., Jiang, G., Wu, D., Sheng, T., Zhou, H., Xu, X., 2014. Nanoscale Zero-Valent Iron (nZVI) assembled on magnetic Fe_3O_4/graphene for Chromium (VI) removal from aqueous solution. J. Colloid Interface Sci. 417, 51–59.
Mahmoud, M.E., Khalifa, M.A., El Wakeel, Y.M., Header, M.S., Abdel-Fattah, T.M., 2017. Engineered nano-magnetic iron oxide-urea-activated carbon nanolayer sorbent for potential removal of uranium (VI) from aqueous solution. J. Nucl. Mater. 487, 13–22.
Manobala, T., Shukla, S.K., Rao, T.S., Kumar, M.D., 2020. Kinetic modelling of the uranium biosorption by deinococcus radiodurans biofilm. Chemosphere 128722.
Mehrabi, N., Masud, A., Afolabi, M., Hwang, J., Calderon Ortiz, G.A., Aich, N., 2019. Magnetic graphene oxide-nano zero valent iron (GO-nZVI) nanohybrids synthesized using biocompatible cross-linkers for methylene blue removal. RSC Adv. 9 (2), 963–973.
Murray, J.S., Politzer, P., 2011. The electrostatic potential: an overview. Wiley Interdisciplinary Reviews: Computational Molecular Science 1 (2), 153–163.
Pavelková, A., Cencerová, V., Zeman, J., Antos, V., Nosek, J., 2020. Reduction of chlorinated hydrocarbons using nano zero-valent iron supported with an electric field. Characterization of electrochemical processes and thermodynamic stability. Chemosphere 128764.
Peng, R., Shao, J., Xie, Y., Chen, A., Peng, L., Zeng, Q., Luo, S., 2017. Oxalate-enhanced reactivity of nanoscale zero-valent iron under different conditions of O_2 , N_2 or without aeration. Chem. Eng. J. 330, 398–406.
Peng, Y., Mu, Y., Xue, C., Chen, A., Peng, L., Wu, H., Luo, S., 2021. Cysteine-enhanced reductive degradation of nitrobenzene using nano-sized zero-valent iron by accelerated electron transfer. J. Environ. Sci. 100, 110–116.
Pirsaheb, M., Moradi, S., Shahlaei, M., Wang, X., Farhadian, N., 2018. A new composite of nano zero-valent iron encapsulated in carbon dots for oxidative removal of bio-refractory antibiotics from water. J. Clean. Prod. 209, 1523–1532.
Raji, M., Mirbagheri, S.A., Ye, F., Dutta, J., 2021. Nano zero-valent iron on activated carbon cloth support as Fenton-like catalyst for efficient color and COD removal from melanoidin wastewater. Chemosphere 263, 127945.
Shenderova, O., Panich, A.M., Moseenkov, S., Hens, S.C., Kuznetsov, V., Vieth, H.-M., 2011. Hydroxylated detonation nanodiamond: FTIR, XPS, and NMR studies. J. Phys. Chem. C 115 (39), 19005–19011.
Singh, P., Pal, P., Mondal, P., Saravanan, G., Nagababu, P., et al., 2021. Kinetics and mechanism of arsenic removal using sulfide-modified nanoscale zerovalent iron. Chem. Eng. J. 412, 128667.
Srirattana, S., Piaowan, K., Lowry, G.V., Phenrat, T., 2017. Electromagnetic induction of foam-based nanoscale zerovalent iron (NZVI) particles to thermally enhance non-aqueous phase liquid (NAPL) volatilization in unsaturated porous media: proof of concept. Chemosphere 183, 323–331.
Stankovich, S., Piner, R.D., Nguyen, S.T., Ruoff, R.S., 2006. Synthesis and exfoliation of isocyanate-treated graphene oxide nanoplatelets. Carbon 44 (15), 3342–3347.
Sun, Y., Ding, C., Cheng, W., Wang, X., 2014. Simultaneous adsorption and reduction of U(VI) on reduced graphene oxide-supported nanoscale zerovalent iron. J. Hazard Mater. 280, 399–408.

Tsarev, S., Collins, R.N., Ilton, E.S., Fahy, A., Waite, T.D., 2017. The short-term reduction of uranium by nanoscale zero-valent iron (nZVI): role of oxide shell, reduction mechanism and the formation of U(v)-carbonate phases. Environ. Sci.: Nano 4 (6), 1304–1313.

Vilardi, G., Di Palma, L., Verdone, N., 2019. A physical-based interpretation of mechanism and kinetics of Cr(VI) reduction in aqueous solution by zero-valent iron nanoparticles. Chemosphere 220, 590–599.

Wang, Q., Masud, A., Aich, N., Wu, Y., 2018. In vitro pulmonary toxicity of reduced graphene oxide-nano zero valent iron nanohybrids and comparison with parent nanomaterial attributes. ACS Sustain. Chem. Eng. 6 (10).

Wu, Y., Li, B., Wang, X., Yu, S., Pang, H., Liu, Y., et al., 2019. Magnetic metal-organic frameworks (Fe_3O_4@ZIF-8) composites for U(VI) and Eu(III) elimination: simultaneously achieve favorable stability and functionality. Chem. Eng. J. 378, 122105.

Xiang, S., Cheng, W., Nie, X., Ding, C., Yi, F., Asiri, A.M., Marwani, H.M., 2018. Zero-valent iron-aluminum for the fast and effective U(VI) removal. Journal of the Taiwan Institute of Chemical Engineers 85, 186–192.

Xiang, S., Cheng, W., Chi, F., Nie, X., Hayat, T., Alharbi, N.S., 2020. Photocatalytic removal of U(VI) from wastewater via synergistic carbon-supported zero-valent iron nanoparticles and S. Putrefaciens. ACS Applied Nano Materials 3 (2), 1131–1138.

Xie, Y., Chen, C., Ren, X., Wang, X., Wang, H., Wang, X., 2019. Emerging natural and tailored materials for uranium-contaminated water treatment and environmental remediation. Prog. Mater. Sci. 103, 180–234.

Xing, R., He, J., Hao, P., Zhou, W., 2020. Graphene oxide-supported nanoscale zero-valent iron composites for the removal of atrazine from aqueous solution. Colloid. Surface. Physicochem. Eng. Aspect. 124466.

Yang, S., Zong, P., Ren, X., Wang, Q., Wang, X., 2012. Rapid and highly efficient preconcentration of Eu(III) by core-shell structured Fe_3O_4@Humic acid magnetic nanoparticles. ACS Appl. Mater. Interfaces 4 (12), 6891–6900.

Ye, Zh, Xu, N., Li, D., Qian, J., Du, Ch, Chen, M., 2021. Vitamin C mediates the activation of green tea extract to modify nanozero-valent iron composites: enhanced transport in heterogeneous porous media and the removal of hexavalent chromium. J. Hazard Mater. 411, 125042.

Yiming, Z., Zhang, H., Liu, Q., Chen, R., Liu, J., Yu, J., et al., 2018. Polypyrrole modified Fe^0-loaded graphene oxide for enrichment of uranium (VI) from simulated seawater. Dalton Trans. 47 (37), 12984–12992.

Yu, S., Wei, D., Shi, L., Ai, Y., Zhang, P., Wang, X., 2019. Three-dimensional graphene/titanium dioxide nanoparticle hybrids for enhanced U(VI) capture: batch, spectroscopy analysis and theoretical calculation. Environ. Pollut. 251, 975–983.

Zhang, J., Liu, Q., Ding, Y., Bei, Y., 2011. 3-aminopropyltriethoxysilane functionalized nanoscale zero-valent iron for the removal of dyes from aqueous solution. Pol. J. Chem. Technol. 13 (2), 35–39.

Zhang, H., Zhang, X., Guo, R., Cheng, Q., Cheng, X., 2018. A facile strategy to fabricate nanoscale zero-valent iron decorated graphene oxide composite for dechloridation of trichloroacetic acid in water. J. Nanosci. Nanotechnol. 18 (12), 8252–8257.

Zhang, W., Qian, L., Ouyang, D., Chen, Y., Han, L., Chen, M., 2019a. Effective removal of Cr(VI) by attapulgite-supported nanoscale zero-valent iron from aqueous solution: enhanced adsorption and crystallization. Chemosphere 221, 683–692.

Zhang, L., Li, Y., Guo, H., Zhang, H., Zhang, N., Hayat, T., Sun, Y., 2019b. Decontamination of U(VI) on graphene oxide/Al_2O_3 composites investigated by XRD, FT-IR and XPS techniques. Environ. Pollut. 248, 332–338.

Zhao, Q., Li, X., Xiao, S., Peng, W., Fan, W., 2020. Integrated remediation of sulfate reducing bacteria and nano zero valent iron on cadmium contaminated sediments. J. Hazard Mater. 124680.